Molecular Imaging and Biology
DOI 10.1007/s11307-022-01720-6

RESEARCH ARTICLE

Preliminary Evaluation of ^{68}Ga-P16-093, a PET Radiotracer Targeting Prostate-Specific Membrane Antigen in Prostate Cancer

Hwan Lee[1], Joshua S. Scheuermann[1], Anthony J. Young[1], Robert K. Doot[1], Margaret E. Daube-Witherspoon[1], Erin K. Schubert[1], Matthew A. Fillare[1], David Alexoff[2], Joel S. Karp[1], Hank F. Kung[2], and Daniel A. Pryma[1]

1Department of Radiology, University of Pennsylvania Perelman School of Medicine, 3400 Spruce Street, Philadelphia, PA 19104, USA
[2]Five Eleven Pharma Inc., Philadelphia, PA 19104, USA 2022

Abstract

Purpose: Prostate-specific membrane antigen (PSMA) is a promising molecular target for imaging of prostate adenocarcinoma. ^{68}Ga-P16-093, a small molecule PSMA ligand, previously showed equivalent diagnostic performance compared to ^{68}Ga-PSMA-11 PET/CT in a pilot study of prostate cancer patients with biochemical recurrence (BCR). We performed a pilot study for further characterization of ^{68}Ga-P16-093 including comparison to conventional imaging.

Procedures: Patients were enrolled into two cohorts. The biodistribution cohort included 8 treated prostate cancer patients without recurrence, who underwent 6 whole body PET/CT scans with urine sampling for dosimetry using OLINDA/EXM. The dynamic cohort included 15 patients with BCR and 2 patients with primary prostate cancer. Two patients with renal cell carcinoma were also enrolled for exploratory use. A dynamic PET/CT was followed by 2 whole body scans for imaging protocol optimization based on bootstrapped replicates. ^{68}Ga-P16-093 PET/CT was compared for diagnostic performance against available ^{18}F-fluciclovine PET/CT, ^{99m}Tc-MDP scintigraphy, diagnostic CT, and MRI.

Results: ^{68}Ga-P16-093 deposited similar effective dose (0.024 mSv/MBq) and lower urinary bladder dose (0.064 mSv/MBq) compared to ^{68}Ga-PSMA-11. The kidneys were the critical organ (0.290 mSv/MBq). While higher injected activities were preferable, lower injected activities at 74–111 MBq (2–3 mCi) yielded 80% retention in signal-to-noise ratio. The optimal injection-to-scan interval was 60 min, with acceptable delay up to 90 min. ^{68}Ga-P16-093 PET/CT showed superior diagnostic performance over conventional imaging with overall patient-level lesion detection rate of 71%, leading to a change in management in 42% of the patients.

Conclusions: Based on its favorable imaging characteristics and diagnostic performance in prostate cancer, ^{68}Ga-P16-093 PET/CT merits further investigation in larger clinical studies.

Key words Prostate-specific membrane antigen · Positron emission tomography computed tomography · Prostate cancer · Biochemical recurrence

Correspondence to: Daniel A. Pryma*; e-mail: DPryma@pennmedicine.upenn.edu*

Published online: 29 March 2022

Introduction

Prostate-specific membrane antigen (PSMA), a transmembrane glycoprotein with glutamate carboxypeptidase activity, is a molecular imaging target under extensive investigation for prostate adenocarcinoma and potentially for renal cell carcinoma (RCC) [1–3]. As a "one-stop-shop" imaging modality for detecting disease in the prostate, lymph nodes, soft tissue, and bone, PSMA PET has demonstrated versatile clinical utility in staging and localization of primary and metastatic disease as well as in theranostic screening [4]. To date, PSMA PET has been mainly studied in the setting of biochemical recurrence (BCR) of prostate cancer, with superior performance compared to conventional imaging modalities such as bone scintigraphy and CT [5]; PSMA PET has also been shown to have utility in newly diagnosed prostate cancer patients [6].

Among at least 25 different PSMA radiotracers under clinical investigation, ^{68}Ga-PSMA-11 is the most extensively studied, demonstrating approximately 90% detection rate and positive predictive value of 84–92% in the setting of BCR [2, 7, 8]. Based on two prospective clinical trials, the US Food and Drug Administration approved ^{68}Ga-PSMA-11 PET for both primary and biochemically recurrent prostate cancer in December 2020 [9]. ^{68}Ga-PSMA-11 is currently undergoing various stages of additional phase III clinical trials for both primary (e.g., NCT02678351) and recurrent (e.g., NCT03822845) prostate cancer. ^{18}F-DCFPyL, also known as ^{18}F-piflufolastat, was the second PSMA PET agent to be approved based on two prospective multi-center clinical trials [6, 10].

Previously, we developed a novel PSMA PET radiotracer ^{68}Ga-P16-093: an O-(carboxymethyl)-L-tyrosine-containing analog of ^{68}Ga-PSMA-11 (Fig. 1) [11]. Compared to ^{68}Ga-PSMA-11, ^{68}Ga-P16-093 demonstrated higher internalization fraction and comparable binding affinity and specificity *in vitro*, resulting in promising *in vivo* biodistribution profile in a mouse prostate cancer model [11]. More recently, a pilot study of ^{68}Ga-P16-093 against ^{68}Ga-PSMA-11 PET/CT in 10 patients with BCR revealed equivalent diagnostic performance and less urinary radiotracer excretion [12].

In this phase I study, we first evaluated the biodistribution and dosimetry profile of ^{68}Ga-P16-093 in post-curative therapy prostate cancer patients without evidence of disease recurrence. We then examined ^{68}Ga-P16-093 uptake in prostate cancer patients with BCR, as well as in patients with primary prostate cancer and RCC. Radiation dose distribution, imaging protocol optimization, and diagnostic performance were investigated to assess the suitability of ^{68}Ga-P16-093 PET/CT for continued development.

Materials and Methods

Study Population

A total of 27 male patients were prospectively enrolled into two separate cohorts. The biodistribution cohort included 8 prostate cancer patients status-post curative prostatectomy and/or radiotherapy without evidence of BCR. BCR was defined as serum prostate-specific antigen (PSA) level $\geq$ 0.2 ng/mL for radical prostatectomy patients and above-nadir PSA level for radiotherapy-only patients, both measured over at least 2 consecutive tests. The patients on androgen deprivation therapy (ADT) within 3 months or with recurrent disease on conventional imaging were excluded. The dynamic cohort mainly consisted of 15 biochemically recurrent prostate cancer patients with known or suspected

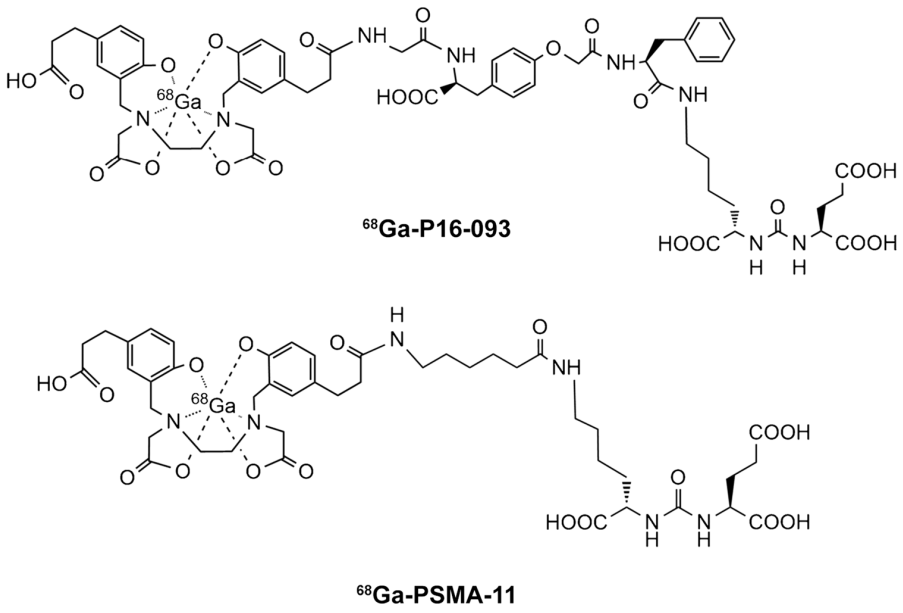

Fig. 1 The chemical structures of ^{68}Ga-P16-093 and ^{68}Ga-PSMA-11.

disease site identified on conventional clinical imaging within 12 months. Two patients with primary prostate cancer and two patients with suspected recurrence of resected clear cell RCC were also included in the dynamic cohort. The key exclusion criteria for both cohorts were estimated creatinine clearance of < 30 ml/min and chemotherapy or radiation therapy within 2 weeks prior to imaging.

Synthesis and Administration of ^{68}Ga-P16-093

^{68}Ga-P16-093 was synthesized with ≥ 95% radiochemical purity using ^{68}Ge/^{68}Ga generators as previously described [11, 12]. The patients received 161 ± 30 MBq (4.4 ± 0.8 mCi) of ^{68}Ga-P16-093 intravenously. The patients were monitored for vital sign abnormalities and clinical symptoms during the study and were followed up for 24 h after radiotracer administration to identify adverse events.

PET/CT Acquisition

For the 8 patients in the biodistribution cohort, 6 whole body PET scans were acquired approximately 1, 20, 40, 60, 120, and 150 min following the radiotracer administration, with 2–3 low-dose CT scans for attenuation correction. For the 19 patients in the dynamic cohort, a dynamic PET over the site of suspected disease with low-dose CT for attenuation correction was acquired for 60 min following the radiotracer administration. Subsequently, two whole body PET scans with low-dose CT were obtained at approximately 90 and 150 min post injection. The scans were obtained using a Philips Ingenuity TF PET/CT scanner (Philips Healthcare, Cleveland, OH, USA). The clinical whole body time-of-flight ordered subset maximum likelihood expectation–maximization algorithm was used for image reconstruction [13].

Biodistribution and Radiation Dosimetry

Total activity residing in the brain, heart, intestines, kidneys, liver, lungs, spleen, gallbladder, salivary glands, and urinary bladder were measured directly from PET images via PMOD v3.7 software (PMOD Technologies, Zürich, Switzerland). Activity in the red marrow was calculated using activity concentrations in lumbar vertebrae 2–4. For accurate estimation of urinary bladder activity, the subjects had opportunities to void after the fourth and sixth PET scans for activity concentration measurement using a 2480 WIZARD^2 gamma counter (PerkinElmer, Waltham, MA, USA). For one patient without urine samples, total activity was estimated using a volume of interest of the upper 50% of activity within the urinary bladder, with the activity concentration decay corrected to the intended time of urine sampling and multiplied by total urine volume to yield total activity of the bladder void.

For radiation dosimetry, time-activity curves for source organs were generated, and the curves were fit to mono- or bi-exponential functions using OLINDA/EXM v1.1 software [14]. For the curves that were poorly modeled by exponential functions, a Riemann Sum was used to calculate numbers of disintegrations occurring in organs during the time period of PET imaging acquisition. To this Riemann sum was added the activity in the organs after the final scan, which was estimated from the area under the curve of a mono-exponential fit of the final points or by assuming physical decay from the final imaging time point to determine the number of disintegrations. Absorbed dose estimates were calculated using OLINDA/EXM v1.1 software using the Standard Adult Male phantom, except for the salivary glands, where OLINDA's unit density sphere model was applied to each salivary gland and reported as average salivary gland absorbed dose [15].

Image Acquisition Optimization

In order to optimize the administered activity and injection-to-scan interval for future applications, the acquired list-mode data from selected 4 patients in the dynamic cohort were replicated 10 times using bootstrapping with replacement [16, 17]. For optimization of administered activity, lower administered activities were simulated by reconstructing only a fraction of the list-mode events from the 90-min post-injection PET/CT. Specifically, 37 and 74 MBq (1 and 2 mCi) doses were considered for all 4 patients; 111 MBq (3 mCi) doses were also simulated for the 2 patients with injected activities above 148 MBq (4 mCi). Lesion maximum uptake (L_{max}) was measured in 1 to 11 regions of focal uptake in each subject. The uptake measurement precision across the 10 replicates was determined as %SD of maximum uptake (SD of L_{max} across replicates divided by the average L_{max}). The signal-to-noise ratio (SNR) was calculated as the reciprocal of %SD for each lesion.

For optimization of injection-to-scan-start interval, the timepoints of 60, 90, and 150 min post-injection were used to calculate the SNR for each lesion, where the 60-min timepoint was generated from the dynamic PET/CT data. Only the lesions visible at all timepoints were included in the analysis, ranging from 1–5 in each subject.

Diagnostic Performance

In the dynamic cohort, each 90-min post injection whole body ^{68}Ga-P16-093 PET/CT was interpreted based on a consensus between two of the authors (H. L. and D. A. P.), taking into account the available diagnostic scans as well as the known physiologic variants and pitfalls of PSMA PET [18–20]. The results were then compared with clinical ^{18}F-fluciclovine PET/CT, ^{99m}Tc-MDP scintigraphy, diagnostic CT, and MRI as available, for which the existing clinical interpretations were adopted following verification. The patient-level lesion detection rate was calculated for ^{68}Ga-P16-093 PET/CT and was compared to serum PSA levels.

For lesion-by-lesion comparison, each lesion found on imaging was classified as benign or malignant based on all available clinical imaging, laboratory values, treatment response, change over time, biopsy results, and assessment by the multidisciplinary care team. For example, a malignant lesion would be confirmed with histopathology, grow on follow-up clinical imaging performed at least 9 months later, or undergo radiotherapy with subsequent decline in PSA. Positive imaging findings were then considered true or false based on concordance with the lesion classification, and the lesion-level sensitivity of ^{68}Ga-P16-093 PET/CT was compared to those of the other clinical imaging modalities.

Statistical Analysis

Descriptive statistics were used for the patient characteristics, biodistribution, radiation dosimetry, SNR, and diagnostic performance. For comparison of SNR across emulated activities and injection-to-scan intervals, one-way repeated measures analysis of variance was used with $\alpha = 0.05$ on GraphPad Prism 8 (GraphPad Software, San Diego, CA, USA).

Results

Patient Characteristics and Safety

The characteristics of the study participants are summarized in Table 1. The median age in the biodistribution cohort was 61 (range 53–80), with median Gleason score of 7 (range 6–9). All patients in the biodistribution cohort received radical prostatectomy with or without radiotherapy, and 5 patients had history of ADT.

In the dynamic cohort, the median age and Gleason score were 71 (range 59–83) and 7 (range 6–9), respectively. The median PSA level and PSA velocity were 5.5 ng/mL (range 0.24–128 ng/mL) and 3.2 ng/ml per year (range 0.73–50 ng/mL per year), respectively. The cohort included 3 patients treated only with curative-intent radiotherapy and 8 patients with history of ADT. The available conventional imaging modalities for comparison were ^{99m}Tc-MDP scintigraphy (13 patients), ^{18}F-fluciclovine PET/CT (9 patients), CT (9 patients), and MRI (9 patients).

Following administration of 129–207 MBq (3.5–5.6 mCi) of ^{68}Ga-P16-093, all patients were discharged safely without vital sign abnormalities or new clinical symptoms. No adverse event occurred within the 24-h follow-up period.

Biodistribution and Radiation Dosimetry

Maximum intensity projection images of ^{68}Ga-P16-093 biodistribution in a representative subject are shown in Fig. 2. Mean ^{68}Ga-P16-093 injected activity percentages in organs as functions of time are shown in Fig. 3. ^{68}Ga-P16-093 activity concentrated in the kidneys, salivary and lacrimal glands, spleen, liver, intestines, and urinary bladder, with the average absorbed-dose estimates summarized in Table 2. The highest individual organ absorbed dose was 0.290 mSv/MBq in the kidneys. The average effective dose was 0.024 ± 0.004 mSv/MBq. An average of 173 MBq (4.68 mCi) injected activity resulted in doses of 50.1 mSv to the kidneys, 17.5 mSv to

Table 1. Characteristics of the study participants

	Biodistribution cohort	Dynamic cohort		
		Recurrent	Primary	RCC
Number of patients	8	15	2	2
Age	61 (53–80)	72 (60–87)	(60–71)	(59–83)
Gleason score	7 (6–9)	7 (6–9)	(6–7)	N/A
PSA (ng/mL)	(undetectable–0.14)	2.1 (0.24–264)	(5.5–128)	N/A
PSA velocity (ng/mL per year)	N/A	2.6 (0.73–250)	(4.3–50)	N/A
Curative intent treatment				
Surgery only	3	7	N/A	2**
Surgery + XRT	5	5	N/A	0
XRT only	0	3	N/A	0
Prior ADT*	5	8	N/A	N/A
Injected activity (MBq)	173 ± 27	155 ± 30	(128–159)	(186–199)
(mCi)	4.7 ± 0.7	4.1 ± 0.8	(3.5–4.3)	(5.0–5.4)
Conventional imaging				
^{18}F-fluciclovine PET/CT	N/A	8	1	0
MRI	N/A	8	1	0
^{99m}Tc-MDP scintigraphy	N/A	11	1	1
CT	N/A	6	1	2

Values are reported as median (range) or mean ± SD

*No patient was on ADT within 3 months of ^{68}Ga-P16-093 PET/CT. **One patient also received adjuvant sunitinib and palliative XRT

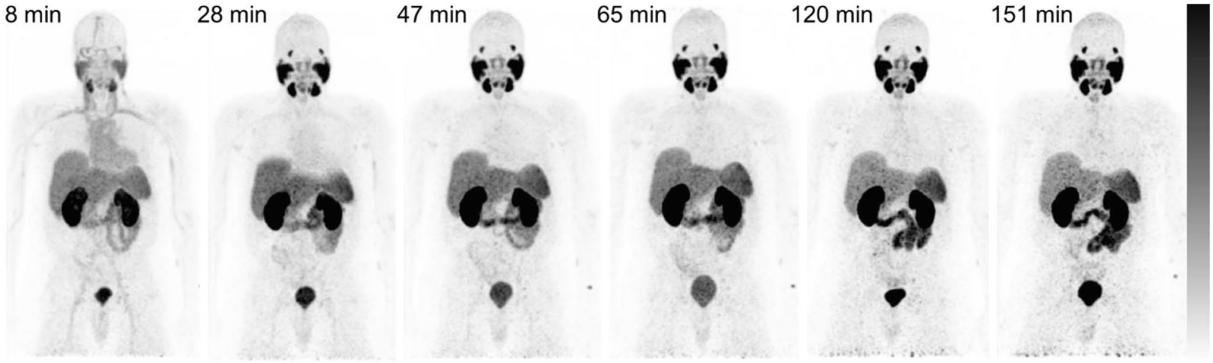

Fig. 2 Coronal maximum intensity projections of ^{68}Ga-P16-093 PET in a biodistribution cohort patient, with scan midpoint times shown in the upper left corners. Images are scaled from 0–12 standardized uptake value (g/mL), decay corrected to the time of injection.

the spleen, and 17.3 mSv to the salivary glands, yielding an effective dose of 4.2 mSv.

Image Acquisition Optimization

As expected, the SNR increased with higher administered activity (Fig. 4a) ($p < 0.0001$). Relative to the SNR calculated from the actual injected activities of 109–165 MBq (2.9–4.5 mCi), an average of 79.9% of the SNR was retained with the simulated activities of 74–111 MBq (2–3 mCi), suggesting that lower injected activities may be acceptable in clinical applications while higher injected activities are preferable.

The SNR decreased at 150 min compared to 90 min post-injection ($p = 0.0006$) primarily due to the physical decay of the ^{68}Ga label, suggesting lack of benefit in imaging later than 90 min (Fig. 4b). While there was no statistical difference in SNR between the 60-min and 90-min timepoints ($p = 0.79$), the average SNR on patient-level was higher at 60-min

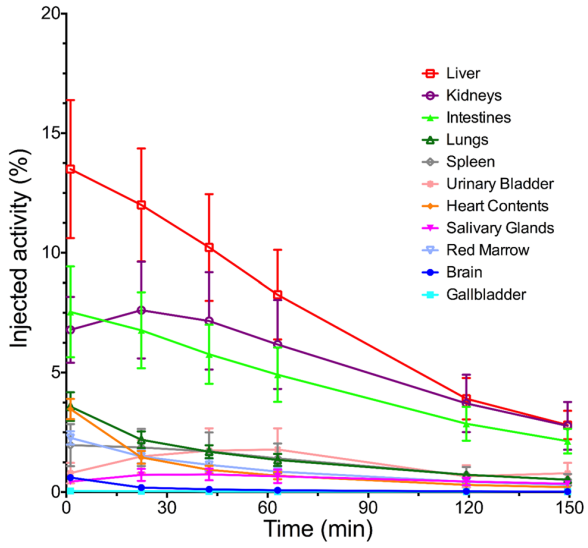

Fig. 3 Mean ^{68}Ga-P16-093 injected activity percentages (± SD) in organs as functions of post-injection time in the 8 patients in the biodistribution cohort (except gallbladder $n = 7$).

Table 2. ^{68}Ga-P16-093 absorbed dose estimates in mSv/MBq for 8 male humans

Target organ	Mean	Standard deviation
Adrenals	1.42E − 02	8.66E − 04
Brain	2.11E − 03	2.09E − 04
Breast	7.53E − 03	4.13E − 04
Gallbladder wall*	1.95E − 02	2.11E − 03
Lower large intestine wall	1.75E − 02	2.34E − 03
Small intestine	6.70E − 02	1.38E − 02
Stomach wall	1.12E − 02	3.62E − 04
Upper large intestine wall	5.09E − 02	9.82E − 03
Heart wall	2.19E − 02	1.81E − 03
Kidneys	2.90E − 01	9.85E − 02
Liver	6.45E − 02	1.28E − 02
Lungs	2.32E − 02	2.77E − 03
Muscle	8.79E − 03	3.47E − 04
Ovaries	1.22E − 02	9.16E − 04
Pancreas	1.40E − 02	4.73E − 04
Red marrow	1.30E − 02	1.20E − 03
Osteogenic cells	1.44E − 02	8.76E − 04
Skin	7.10E − 03	3.72E − 04
Spleen	1.01E − 01	4.01E − 02
Testes	7.78E − 03	4.44E − 04
Thymus	8.48E − 03	4.70E − 04
Thyroid	7.56E − 03	5.10E − 04
Urinary bladder wall**	6.41E − 02	1.98E − 02
Uterus	1.23E − 02	8.36E − 04
Salivary glands***	9.97E − 02	3.60E − 02
Total body	1.29E − 02	3.04E − 04
Effective dose equivalent	4.47E − 02	4.71E − 03
Effective dose	2.43E − 02	3.83E − 03

*Gallbladder results do not include one subject who had cholecystectomy ($n = 7$). **Urinary bladder wall dose based on bladder voiding interval of 2.4 h. ***Salivary glands absorbed dose calculation based on Herrmann et al. [15]

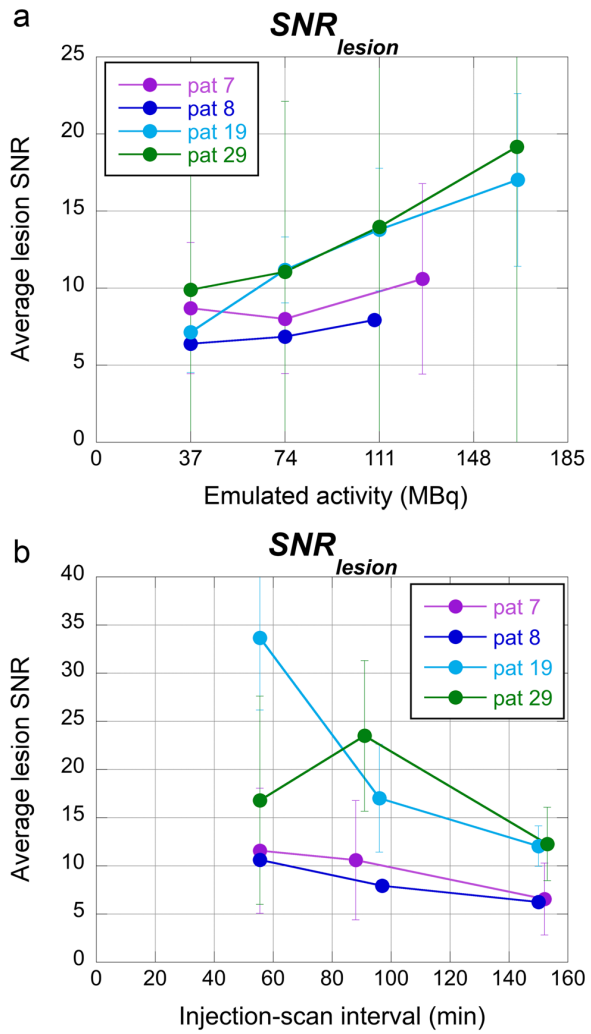

Fig. 4 Image acquisition optimization based on bootstrapped replicates for 4 patients. (**a**) The effect of injected activity on the lesion SNR. (**b**) The effect of injection-scan interval on the lesion SNR.

post-injection for 3 of the 4 patients. Therefore, the choice of 60 min for injection-to-scan interval would be reasonable, without significant loss of SNR up to 90 min post-injection.

Diagnostic Performance

Among the 17 prostate cancer patients in the dynamic cohort, ^{68}Ga-P16-093 PET/CT was positive in 12 patients, yielding the lesion detection rate of 71% (Table 3). The detection rate was 25% when PSA was ≤ 0.5 ng/mL, 67% when PSA was > 0.5 ng/mL and ≤ 2.0 ng/mL, and 90% when PSA was > 2.0 ng/mL. On lesion-based analysis, ^{68}Ga-P16-093 PET/CT was positive in 66 out of 72 lesions (92% sensitivity) without false positive findings. All of the 6 missed lesions

Table 3. Diagnostic performance of ^{68}Ga-P16-093 PET/CT in the dynamic cohort

	Recurrent PCa	Primary PCa	RCC
Number of patients	15	2	2
Patient-level detection rate	67% (10/15)	100% (2/2)	100% (1/1)*
PSA ≤ 0.5 ng/mL	25% (1/4)	-	-
PSA > 0.5 and ≤ 2.0 ng/mL	67% (2/3)	-	-
PSA > 2.0 ng/mL	88% (7/8)	100% (2/2)	-
Change in management	4	2	2
Lesion-level sensitivity			
Prostate	33% (2/6)	100% (2/2)	-
Regional node	86% (12/14)	100% (6/6)	-
Distant soft tissue	100% (23/23)	-	100% (4/4)
Bone	100% (21/21)	-	-
False positive findings	0	0	0
True negative findings (comparison)			
Bone	6 (fluciclovine)	0	2 (CT)
Regional node	1 (MRI)	0	0
Distant soft tissue	1 (CT)	0	0

*One patient with suspected recurrence was disease-free on follow-up

were loco-regional, 4 in the prostatectomy bed and 2 in the regional lymphatics. Nevertheless, ^{68}Ga-P16-093 PET/CT correctly identified both cases of primary prostate cancer. Although ^{68}Ga-P16-093 PET/CT was not used as a basis for treatment, and no official interpretation was issued, 6 prostate cancer patients had change in management in agreement with the PET/CT findings after further diagnostic workup.

^{18}F-fluciclovine PET/CT was available for comparison in 9 patients with 28 malignant lesions, acquired 107 ± 116 days before or after ^{68}Ga-P16-093 PET/CT (mean ± SD). While ^{18}F-fluciclovine PET/CT was positive in all 9 patients, ^{68}Ga-P16-093 PET/CT showed improved per-lesion sensitivity of 83% (24 out of 28 lesions) without false positive findings compared to 61% for ^{18}F-fluciclovine PET/CT (Fig. 5a). Two of the missed lesions were in the prostatectomy bed, and the remaining two were in pelvic lymph nodes. In addition, ^{68}Ga-P16-093 PET/CT was able to exclude 6 benign osseous lesions found on ^{18}F-fluciclovine PET/CT (Fig. 5b); five of them were not identified on subsequent clinical imaging and one patient's PSA became undetectable after salvage radiation to the prostatectomy bed without treatment of the putative bone lesion.

^{99m}Tc-MDP scintigraphy was available in 5 patients with 20 osseous metastases, acquired 46 ± 21 days before or after ^{68}Ga-P16-093 PET/CT. ^{68}Ga-P16-093 PET/CT was positive in all 20 metastases without false positive findings. In comparison, ^{99m}Tc-MDP scintigraphy identified 16 lesions as positive; two of the missed lesions were successfully treated with salvage radiation, and the remaining two missed lesions were identified on future ^{99m}Tc-MDP scintigraphy (Fig. 5c). Of note, the remaining 7 patients who had ^{99m}Tc-MDP scintigraphy did not have osseous metastases.

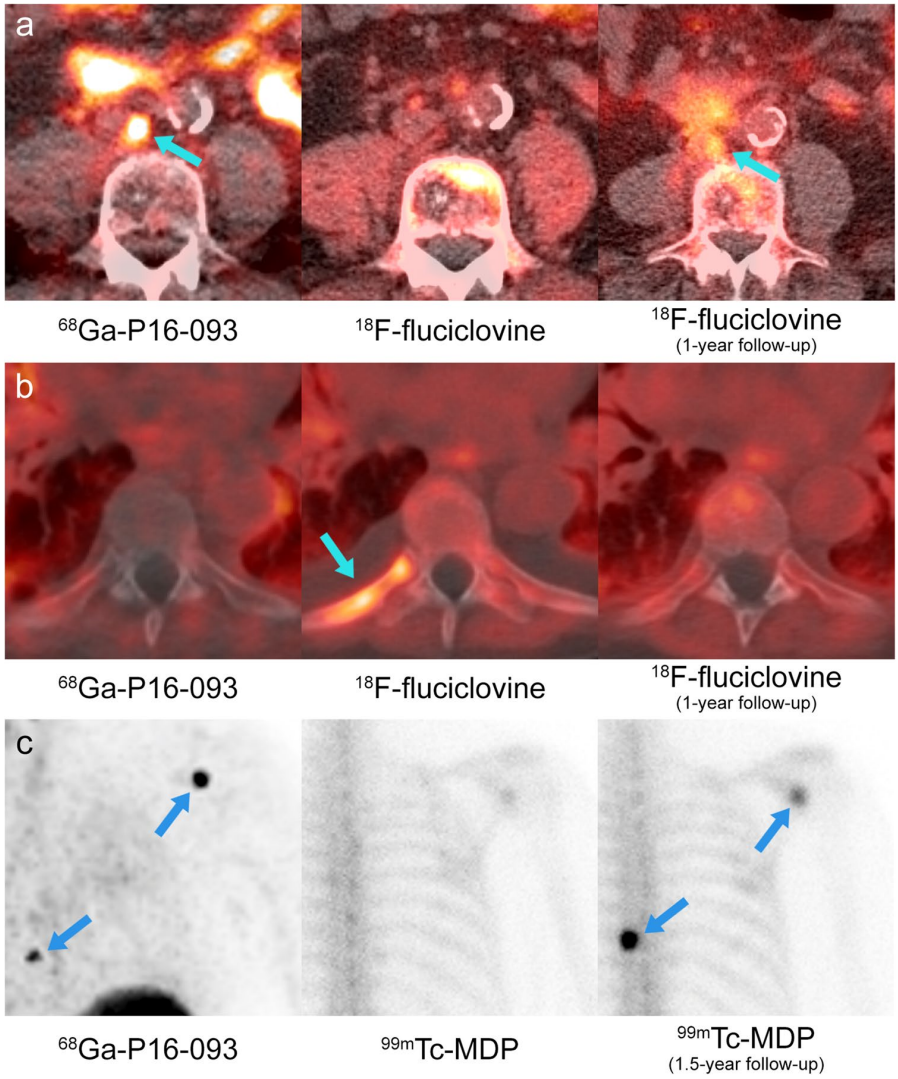

Fig. 5 Diagnostic utility of ^{68}Ga-P16-093 compared to ^{18}F-fluciclovine and ^{99m}Tc-MDP. (**a**) A positive aorto-caval lymph node (arrow) on ^{68}Ga-P16-093 PET/CT did not show appreciable uptake on ^{18}F-fluciclovine PET/CT. After 1 year without treatment, the lymph node demonstrated interval growth in size with fluciclovine uptake. (**b**) In the same patient, no significant ^{68}Ga-P16-093 uptake was seen at the right posterior 8th rib despite suspicious asymmetric uptake (arrow) on ^{18}F-fluciclovine PET/CT. The uptake was resolved on follow-up ^{18}F-fluciclovine PET/CT, and no corresponding focal uptake was seen on ^{99m}Tc-MDP scintigraphy (not shown). (**c**) A posterior maximum intensity projection image of ^{68}Ga-P16-093 PET illustrates right scapular and thoracic vertebral metastases (arrows) in another patient with metastatic prostate cancer. The osseous metastases were not conspicuous on initial ^{99m}Tc-MDP scintigraphy, but later showed intense ^{99m}Tc-MDP uptake (arrows) with disease progression.

In the subgroup of patients with available diagnostic CT and/or MRI, the lesion detection rates for CT and MRI were 29% (2 out of 7 patients) and 56% (5 out of 9 patients), respectively. Although MRI offered better lesion detection rate than CT, it failed to identify both cases of prostate bed recurrence also missed on ^{68}Ga-P16-093 PET/CT; one patient was successfully treated with salvage radiation, and the other patient showed local recurrence on imaging 3 years later. ^{68}Ga-P16-093 PET/CT was useful for further assessment of the non-specific findings made on anatomic imaging (Fig. 6a), while also identifying additional lesions (Fig. 6b) and offering a greater field of view (Fig. 6c).

^{68}Ga-P16-093 PET/CT provided diagnostic value in the two patients with history of RCC. In the first patient with suspected osteoblastic recurrence on CT, ^{68}Ga-P16-093 PET/CT was negative, and the lesion remained stable on future CT (Fig. 7a). In the second patient with previously irradiated rib recurrence and suspicious pulmonary nodules on CT, ^{68}Ga-P16-093 PET/CT was negative in the irradiated lesion and positive in the lung nodules, which demonstrated subsequent growth. In addition, ^{68}Ga-P16-093 PET/CT identified occult pancreatic metastases, the presence of which was confirmed on future CT (Fig. 7b).

Discussion

Here, we report the second pilot study for further characterization of the novel PSMA radiotracer ^{68}Ga-P16-093. Compared to the prior study, we recruited an independent patient population in two cohorts and diversified the analyses to encompass biodistribution, radiation dosimetry, image acquisition optimization, and evaluation of diagnostic utility

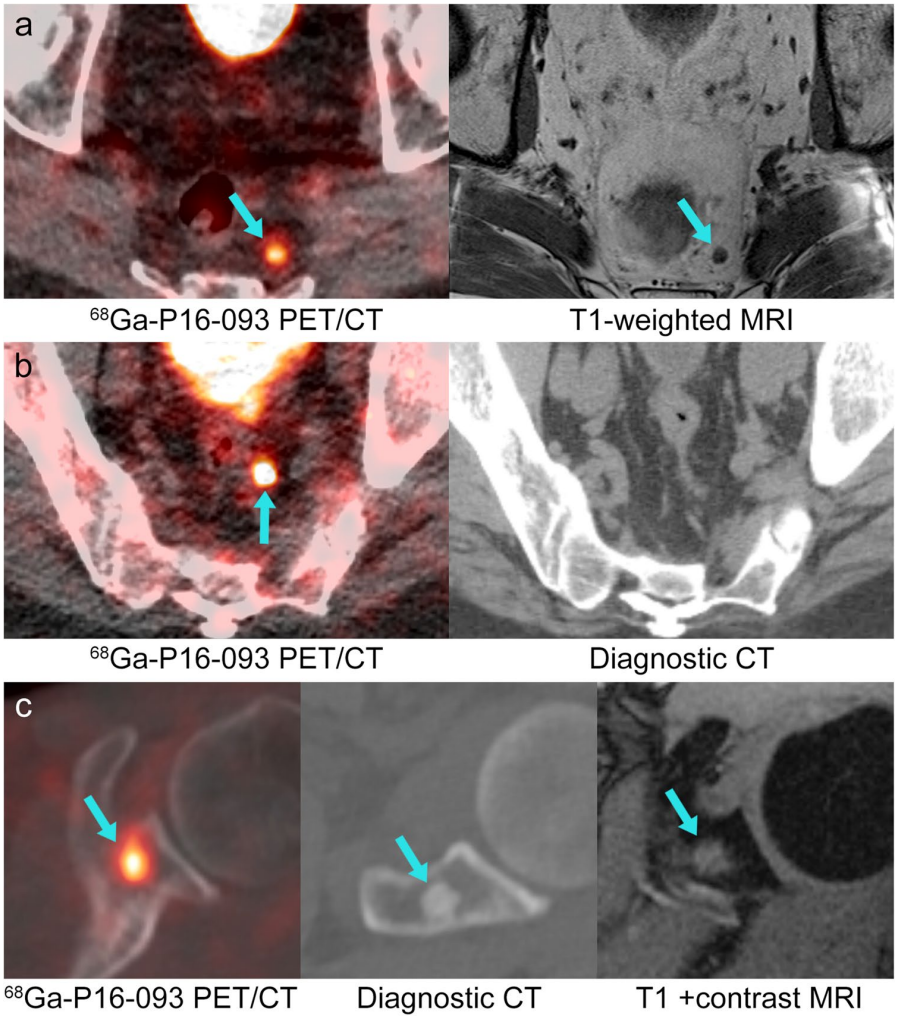

Fig. 6 Diagnostic utility of ^{68}Ga-P16-093 PET/CT compared to diagnostic CT and MRI. (**a**) In a prostate cancer patient with biochemical recurrence, ^{68}Ga-P16-093 PET/CT suggested tumor involvement in a perirectal lymph node (arrow) previously found on MRI. (**b**) In a newly diagnosed prostate cancer patient, ^{68}Ga-P16-093 PET/CT demonstrated tumor spread to a pelvic lymph node (arrow), which was not identified on diagnostic CT performed 2 days earlier. (**c**) After a negative prostate MRI (not shown) was obtained for biochemical recurrence, ^{68}Ga-P16-093 PET/CT showed a focal area of uptake within the left scapula (arrow). Further diagnostic workup with CT and MRI of the chest revealed associated sclerosis and contrast enhancement, respectively (arrows). The lesion was subsequently treated with stereotactic body radiotherapy.

including exploratory use in patients with primary prostate cancer and RCC.

The overall biodistribution profile of ^{68}Ga-P16-093 was similar to those of other ^{68}Ga-PSMA PET agents including ^{68}Ga-PSMA-11 [15, 21–24], with comparable effective dose (Table 4). As reported previously, ^{68}Ga-P16-093 deposited lower radiation dose to the urinary bladder compared to ^{68}Ga-PSMA-11 [12], but its clinical importance and validity across different scanners remain unclear. Despite the lower urinary excretion, the kidneys were the critical organ with the estimated radiation dose of 2.90×10^{-1} mSv/MBq. While the reported effective dose of ^{18}F-DCFPyL (1.16×10^{-2} mSv/MBq) appears lower than that of ^{68}Ga-P16-093, the higher recommended administered activity of ^{18}F-DCFPyL at 333 MBq (9 mCi) leads to comparable radiation dose per scan [25]. The dosimetry results we obtained were similar to those of the prior pilot study, with the effective dose of 2.43×10^{-2} mSv/MBq vs. 2.30×10^{-2} mSv/MBq [12]. The differences in the patient population, technical parameters, and dosimetry methods between the two pilot studies support the generalizability of ^{68}Ga-P16-093 biodistribution and dosimetry results to various clinical settings.

We verified the absence of acute adverse events following intravenous ^{68}Ga-P16-093 administration. Beyond the immediate safety profile, there is also a general concern from both oncologists and patients regarding repeated radiation exposure from cancer monitoring [26]. The retention of SNR at ^{68}Ga-P16-093 doses of 74–111 MBq (2–3 mCi) allows minimization of radiation exposure compared to the clinically used ^{68}Ga-PSMA-11 dose of 111 MBq to 259 MBq (3–7 mCi) [24]. Given that prostate cancer patients may undergo imaging as often as every 12 months or sooner if needed [27], use of lower administered radioactivity would confer cumulative reduction in radiation exposure over the treatment course of a given patient. From a logistical perspective, the optimal ^{68}Ga-P16-093 injection-to-scan interval of 60 min with acceptable delay up to 90 min is similar to

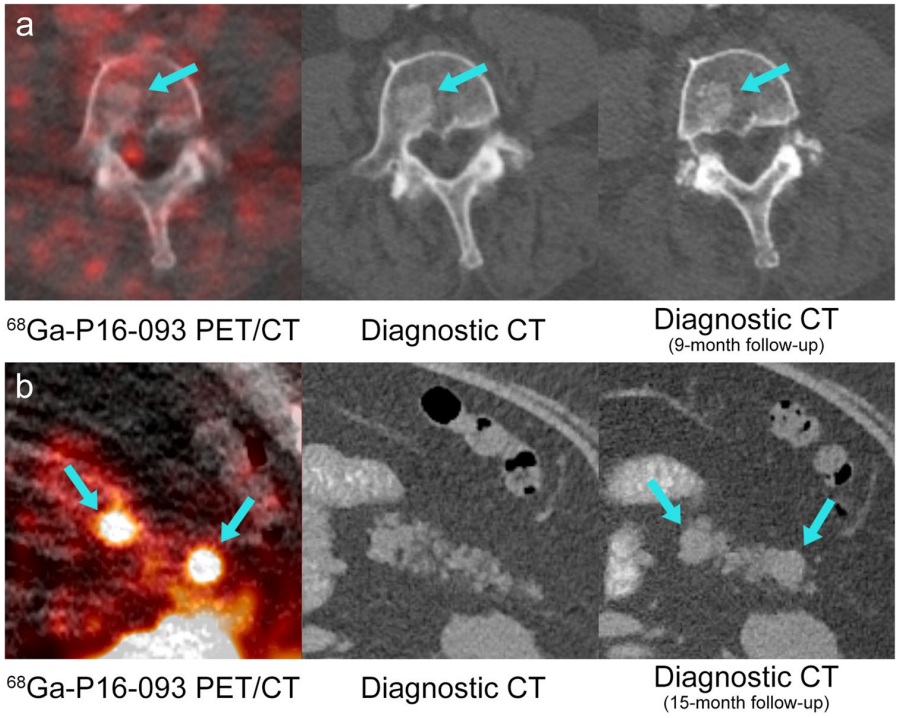

Fig. 7 Diagnostic utility of ^{68}Ga-P16-093 PET/CT in renal cell carcinoma (RCC). (**a**) In a patient with RCC status post partial nephrectomy, ^{68}Ga-P16-093 PET/CT did not show increased uptake at the site of suspected osseous recurrence in the L4 vertebral body (arrow). The osseous lesion was stable (arrow) on follow-up CT. (**b**) In another patient with metastatic RCC, ^{68}Ga-P16-093 PET/CT showed two focal sites of uptake in the pancreas (arrows), which were not identified on previous diagnostic CT. Two pancreatic nodules (arrows) were identified on follow-up CT 15 months later.

Table 4. Comparison of select regional ^{68}Ga-PSMA PET absorbed dose estimates (mSv/MBq)

Target organ	P16-093	PSMA-11 [24]	PSMA-11 [23]	PSMA-11 [21]	PSMA-I&T [15]	PSMA-617 [22]
Kidneys	0.290	0.371	0.262	0.122	0.220	0.206
Spleen	0.101	0.065	0.045	0.043	0.063	0.029
Salivary glands	0.100	-	-	-	0.061	-
Small intestine	0.067	0.014	0.016	0.056	0.011	0.018
Liver	0.065	0.041	0.031	0.021	0.043	0.029
Urinary bladder	0.064	0.098	0.130	0.173	0.067	0.090
Effective dose	0.024	0.017	0.024	0.017	0.020	0.021

the current ^{68}Ga-PSMA-11 imaging protocol [24] and can be easily integrated into the existing clinical workflow using 60-min injection-to-scan interval for ^{18}F-fluorodeoxyglucose PET/CT [28].

The higher diagnostic performance of ^{68}Ga-P16-093 PET/CT compared to ^{18}F-fluciclovine PET/CT, ^{99m}Tc-MDP scintigraphy, and anatomic imaging is in keeping with the now established superiority of PSMA PET over conventional imaging in BCR [29, 30]. In addition to providing higher lesion detection rates, ^{68}Ga-P16-093 PET/CT was particularly useful at further evaluation of osseous ^{18}F-fluciclovine uptake and indeterminate anatomic imaging findings. The lesion detection rates for BCR we found with ^{68}Ga-P16-093 at various levels of PSA (Table 3) were similar to those of ^{68}Ga-PSMA-11 in the literature [7, 31]. Despite the lower urinary excretion of ^{68}Ga-P16-093, adjacent urinary bladder activity remained as an impediment to detection of local recurrence following radical prostatectomy. The other missed lesions were located in the pelvic lymph nodes, a known area of variable sensitivity on PSMA PET [32, 33].

PSMA PET has also demonstrated value in evaluation of newly diagnosed prostate cancer with superior diagnostic accuracy compared to conventional imaging [33–35]. In our experimental use of ^{68}Ga-P16-093 PET/CT in two patients with primary prostate cancer, the primary lesion was identified in both patients and additional pelvic lymph nodes were also found. PSMA PET has also been investigated in RCC, initially for detection of metastatic lesions [36, 37], and more recently for radiologic-pathologic correlation of primary tumors [38, 39]. In our two patients with RCC, ^{68}Ga-P16-093 PET/CT showed diagnostic value in detection of occult metastases and exclusion of possible recurrence. Overall, the change in management among 8 patients (42%) in the dynamic cohort following ^{68}Ga-P16-093 PET/CT, despite its investigational use, is consistent with the existing PSMA PET literature and supports its translation to clinical use [5].

Although the clinical utility of PSMA PET was demonstrated in multiple high-quality trials, its adoption outside of academic institutions has been slow. An advantage of ^{68}Ga-P16-093 is the generator-based production of ^{68}Ga, in contrast to an ^{18}F-based compound which requires a cyclotron for production [40]. Furthermore, ^{68}Ga-P16-093 can be reproducibly prepared using a single kit, which yields clinical doses in 5 min upon simple addition of the ^{68}Ga eluent obtained from a commercial ^{68}Ge/^{68}Ga generator [41]. We envision that the convenient kit-based preparation of ^{68}Ga-P16-093 using a generator would facilitate its adoption by imaging centers in various care settings.

Our study has several limitations. There was considerable variation in SNR among the lesions, which was possibly confounded by partial volume effects for small lesions. For imaging protocol optimization, only the timepoints relevant to existing oncologic PET/CT clinical workflow were examined. The dynamic cohort population was heterogeneous with respect to available clinical imaging, limiting direct comparison of ^{68}Ga-P16-093 PET/CT to conventional imaging in a controlled setting. Also, histopathologic confirmation was not required for our lesion classification. While the patients were not on ADT for at least 3 months before ^{68}Ga-P16-093 PET/CT, prior ADT in a subset of patients acts as a potential confounder. Finally, both patients with RCC had the clear cell subtype by chance, and the utility of ^{68}Ga-P16-093 PET/CT in other RCC subtypes remains to be investigated.

Conclusion

In this two-cohort preliminary study, ^{68}Ga-P16-093 PET/CT demonstrated superior diagnostic accuracy compared to conventional imaging in prostate and renal cell cancer, comparable to the performance of ^{68}Ga-PSMA-11 PET/CT in the literature. Low urinary excretion and SNR retention at low administered activities are its notable features. Its optimal imaging timepoint of 60 min with acceptable delay up to 90 min is conducive to integration into existing PET/CT workflows. Based on its favorable imaging characteristics and diagnostic performance, ^{68}Ga-P16-093 PET/CT merits further investigation in larger clinical studies.

Funding Funding support for the work was received from Five Eleven Pharma. Five Eleven Pharma's development and synthesis of ^{68}Ga-P16-093 were supported by NIH/NCI SBIR grants 1R44CA233140-01 and 1R43CA217425-01.

Declarations

Ethical Approval The University of Pennsylvania Institutional Review Board approved the study. All the procedures performed involving human participants were in accordance with the ethical standards of the institutional research committee and with the 1964 Helsinki declaration and its later amendments or comparable ethical standards.

Informed Consent Informed consent was obtained from all the individual participants included in the study.

Conflict of Interest David Alexoff: CEO of Five Eleven Pharma Inc.
Hank F. Kung: Founder and Chairman of the board at Five Eleven Pharma Inc.
Daniel A. Pryma: Research Consultant, Five Eleven Pharma Inc.; Research Consultant, Progenics Pharmaceuticals Inc.; Research Consultant, Actinium Pharmaceuticals Inc.; Research Consultant, Ipsen; Research Grant, Siemens AG; Research Grant, Five Eleven Pharma Inc.; Research Grant, Progenics Pharmaceuticals Inc.; Clinical Trial Funding, Nordic Nanovector ASA.
The other authors declare that they have no conflict of interest.

References

1. Davis MI, Bennett MJ, Thomas LM, Bjorkman PJ (2005) Crystal structure of prostate-specific membrane antigen, a tumor marker and peptidase. Proc Natl Acad Sci U S A 102:5981–5986
2. Zippel C, Ronski SC, Bohnet-Joschko S, Giesel FL, Kopka K (2020) Current status of PSMA- radiotracers for prostate cancer: data analysis of prospective trials listed on ClinicalTrials.gov. Pharmaceuticals (Basel) 13:12
3. Rhee H, Blazak J, Tham CM et al (2016) Pilot study: use of gallium-68 PSMA PET for detection of metastatic lesions in patients with renal tumour. EJNMMI Res 6:76
4. Hofman MS, Hicks RJ, Maurer T, Eiber M (2018) Prostate-specific membrane antigen PET: clinical utility in prostate cancer, normal patterns, pearls, and pitfalls. Radiographics 38:200–217
5. Han S, Woo S, Kim YJ, Suh CH (2018) Impact of (68)Ga-PSMA PET on the management of patients with prostate cancer: a systematic review and meta-analysis. Eur Urol 74:179–190
6. Pienta KJ, Gorin MA, Rowe SP et al (2021) A phase 2/3 prospective multicenter study of the diagnostic accuracy of prostate specific membrane antigen PET/CT with (18)F-DCFPyL in prostate cancer patients (OSPREY). J Urol 206:52–61
7. Fendler WP, Calais J, Eiber M et al (2019) Assessment of 68Ga-PSMA-11 PET accuracy in localizing recurrent prostate cancer: a prospective single-arm clinical trial. JAMA Oncol 5:856–863
8. Eiber M, Maurer T, Souvatzoglou M et al (2015) Evaluation of hybrid (6)(8)Ga-PSMA ligand PET/CT in 248 patients with biochemical recurrence after radical prostatectomy. J Nucl Med 56:668–674
9. U.S. Food and Drug Administration. Drug trials snapshot: Ga 68 PSMA-11. www.fda.gov/drugs/drug-approvals-and-databases/drug-trials-snapshot-ga-68-psma-11. Accessed 6 Mar 2021
10. Morris MJ, Rowe SP, Gorin MA et al (2021) Diagnostic performance of (18)F-DCFPyL-PET/CT in men with biochemically recurrent prostate cancer: results from the CONDOR Phase III, multicenter study. Clin Cancer Res 27:3674–3682
11. Zha Z, Ploessl K, Choi SR, Wu Z, Zhu L, Kung HF (2018) Synthesis and evaluation of a novel urea-based (68)Ga-complex for imaging PSMA binding in tumor. Nucl Med Biol 59:36–47
12. Green MA, Hutchins GD, Bahler CD et al (2020) [(68)Ga]Ga-P16-093 as a PSMA-targeted PET radiopharmaceutical for detection of cancer: initial evaluation and comparison with [(68)Ga]Ga-PSMA-11 in prostate cancer patients presenting with biochemical recurrence. Mol Imaging Biol 22:752–763
13. Kolthammer JA, Su KH, Grover A, Narayanan M, Jordan DW, Muzic RF (2014) Performance evaluation of the Ingenuity TF PET/CT scanner with a focus on high count-rate conditions. Phys Med Biol 59:3843–3859
14. Stabin MG, Sparks RB, Crowe E (2005) OLINDA/EXM: the second-generation personal computer software for internal dose assessment in nuclear medicine. J Nucl Med 46:1023–1027
15. Herrmann K, Bluemel C, Weineisen M et al (2015) Biodistribution and radiation dosimetry for a probe targeting prostate-specific membrane antigen for imaging and therapy. J Nucl Med 56:855–861
16. Haynor DR, Woods SD (1989) Resampling estimates of precision in emission tomography. IEEE Trans Med Imaging 8:337–343

17. Dahlbom M (2002) Estimation of image noise in PET using the bootstrap method. IEEE Trans Nucl Sci 49:2062–2066
18. Demirci E, Sahin OE, Ocak M, Akovali B, Nematyazar J, Kabasakal L (2016) Normal distribution pattern and physiological variants of 68Ga-PSMA-11 PET/CT imaging. Nucl Med Commun 37:1169–1179
19. Shetty D, Patel D, Le K, Bui C, Mansberg R (2018) Pitfalls in gallium-68 PSMA PET/CT interpretation-a pictorial review. Tomography 4:182–193
20. Ceci F, Oprea-Lager DE, Emmett L et al (2021) E-PSMA: the EANM standardized reporting guidelines v1.0 for PSMA-PET. Eur J Nucl Med Mol Imaging 48:1626–1638
21. Pfob CH, Ziegler S, Graner FP et al (2016) Biodistribution and radiation dosimetry of (68)Ga-PSMA HBED CC-a PSMA specific probe for PET imaging of prostate cancer. Eur J Nucl Med Mol Imaging 43:1962–1970
22. Afshar-Oromieh A, Hetzheim H, Kratochwil C et al (2015) The theranostic PSMA ligand PSMA-617 in the diagnosis of prostate cancer by PET/CT: biodistribution in humans, radiation dosimetry, and first evaluation of tumor lesions. J Nucl Med 56:1697–1705
23. Afshar-Oromieh A, Hetzheim H, Kubler W et al (2016) Radiation dosimetry of (68)Ga-PSMA-11 (HBED-CC) and preliminary evaluation of optimal imaging timing. Eur J Nucl Med Mol Imaging 43:1611–1620
24. U.S. Food and Drug Administration. Gallium Ga 68 PSMA-11 injection, for intravenous use [prescribing information]. Revised December 2020. www.accessdata.fda.gov/drugsatfda_docs/label/2020/212642s000lbl.pdf. Accessed August 27, 2021
25. U.S. Food and Drug Administration. PYLARIFY® (piflufolastat F 18) injection, for intravenous use [prescribing information]. www.accessdata.fda.gov/drugsatfda_docs/label/2021/214793s000lbl.pdf. Accessed January 2, 2022
26. Burke LM, Bashir MR, Neville AM, Nelson RC, Jaffe TA (2014) Current opinions on medical radiation: a survey of oncologists regarding radiation exposure and dose reduction in oncology patients. J Am Coll Radiol 11:490–495
27. National Comprehensive Cancer Network. Clinical practice guidelines in oncology: prostate cancer (Version 2.2021). www.nccn.org/professionals/physician_gls/pdf/prostate.pdf. Accessed August 27, 2021
28. Boellaard R, Delgado-Bolton R, Oyen WJ et al (2015) FDG PET/CT: EANM procedure guidelines for tumour imaging: version 2.0. Eur J Nucl Med Mol Imaging 42:328–354
29. Tan N, Oyoyo U, Bavadian N et al (2020) PSMA-targeted radiotracers versus (18)F fluciclovine for the detection of prostate cancer biochemical recurrence after definitive therapy: a systematic review and meta-analysis. Radiology 296:44–55
30. Yuminaga Y, Rothe C, Kam J et al (2021) (68)Ga-PSMA PET/CT versus CT and bone scan for investigation of PSA failure post radical prostatectomy. Asian J Urol 8:170–175
31. Hope TA, Goodman JZ, Allen IE, Calais J, Fendler WP, Carroll PR (2019) Metaanalysis of (68)Ga-PSMA-11 PET accuracy for the detection of prostate cancer validated by histopathology. J Nucl Med 60:786–793
32. Petersen LJ, Zacho HD (2020) PSMA PET for primary lymph node staging of intermediate and high-risk prostate cancer: an expedited systematic review. Cancer Imaging 20:10
33. Hope TA, Eiber M, Armstrong WR et al (2021) Diagnostic accuracy of 68Ga-PSMA-11 PET for pelvic nodal metastasis detection prior to radical prostatectomy and pelvic lymph node dissection: a multicenter prospective phase 3 imaging trial. JAMA Oncol 7:1635–1642
34. Hofman MS, Lawrentschuk N, Francis RJ et al (2020) Prostate-specific membrane antigen PET-CT in patients with high-risk prostate cancer before curative-intent surgery or radiotherapy (proPSMA): a prospective, randomised, multicentre study. Lancet 395:1208–1216
35. Lopci E, Saita A, Lazzeri M et al (2018) (68)Ga-PSMA positron emission tomography/computerized tomography for primary diagnosis of prostate cancer in men with contraindications to or negative multiparametric magnetic resonance imaging: a prospective observational study. J Urol 200:95–103
36. Raveenthiran S, Esler R, Yaxley J, Kyle S (2019) The use of (68)Ga-PET/CT PSMA in the staging of primary and suspected recurrent renal cell carcinoma. Eur J Nucl Med Mol Imaging 46:2280–2288
37. Sawicki LM, Buchbender C, Boos J et al (2017) Diagnostic potential of PET/CT using a (68)Ga-labelled prostate-specific membrane antigen ligand in whole-body staging of renal cell carcinoma: initial experience. Eur J Nucl Med Mol Imaging 44:102–107
38. Gao J, Xu Q, Fu Y et al (2021) Comprehensive evaluation of (68)Ga-PSMA-11 PET/CT parameters for discriminating pathological characteristics in primary clear-cell renal cell carcinoma. Eur J Nucl Med Mol Imaging 48:561–569
39. Gühne F, Seifert P, Theis B, Steinert M, Freesmeyer M, Drescher R (2021) PSMA-PET/CT in patients with recurrent clear cell renal cell carcinoma: histopathological correlations of imaging findings. Diagnostics (Basel) 11:1142
40. Fani M, André JP, Maecke HR (2008) 68Ga-PET: a powerful generator-based alternative to cyclotron-based PET radiopharmaceuticals. Contrast Media Mol Imaging 3:67–77
41. Hong H, Wang G, Ploessl K et al (2021) Kit-based preparation of [(68)Ga]Ga-P16-093 (PSMA-093) using different commercial (68)Ge/(68)Ga generators. Nucl Med Biol 106–107:1–9